Brain Research 1796 (2022) 148097

Contents lists available at ScienceDirect

Brain Research

journal homepage: www.elsevier.com/locate/brainres

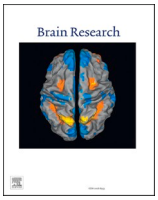

Cerebral metabolic rate of oxygen ($CMRO_2$) changes measured with simultaneous tDCS-MRI in healthy adults

Marco Muccio [a], Lillian Walton Masters [b], Giuseppina Pilloni [b], Peidong He [a], Lauren Krupp [b], Abhishek Datta [c], Marom Bikson [d], Leigh Charvet [b], Yulin Ge [a,*]

[a] Department of Radiology, NYU Grossman School of Medicine, New York City, NY, United States
[b] Department of Neurology, NYU Grossman School of Medicine, New York City, NY, United States
[c] Research and Development, Soterix Medical, Inc, Woodbridge, NJ, United States
[d] Department of Biomedical Engineering, City College of New York, New York City, NY, United States

ARTICLE INFO

Keywords:
Simultaneous transcranial direct current stimulation (tDCS)
MRI
Cerebral blood flow (CBF)
Cerebral metabolic rate of oxygen ($CMRO_2$)
Healthy adults
Neuronal activity

ABSTRACT

Background: Transcranial direct current stimulation (tDCS) is a safe and well-tolerated noninvasive technique used for cortical excitability modulation. tDCS has been extensively investigated for its clinical applications; however further understanding of its underlying *in-vivo* physiological mechanisms remains a fundamental focus of current research.

Objectives: We investigated the simultaneous effects of tDCS on cerebral blood flow (CBF), venous blood oxygenation (Yv) and cerebral metabolic rate of oxygen ($CMRO_2$) using simultaneous MRI in healthy adults to provide a reference frame for its neurobiological mechanisms.

Methods: Twenty-three healthy participants (age = 35.6 ± 15.0 years old, 10 males) completed a simultaneous tDCS-MRI session in a 3 T scanner fitted with a 64-channels head coil. A MR-compatible tDCS device was used to acquire CBF, Yv and $CMRO_2$ at three time points: pre-, during- and post- 15 minutes of 2.0 mA tDCS on left anodal dorsolateral prefrontal cortex.

Results: During tDCS, CBF significantly increased (57.10 ± 8.33 mL/100g/min) from baseline (53.67 ± 7.75 mL/100g/min; $p < 0.0001$) and remained elevated in post-tDCS (56.79 ± 8.70 mL/100g/min). Venous blood oxygenation levels measured in pre-tDCS (60.71 ± 4.12 %) did not significantly change across the three time-points. The resulting $CMRO_2$ significantly increased by 5.9 % during-tDCS (175.68 ± 30.78 μmol/100g/min) compared to pre-tDCS (165.84 ± 25.32 μmol/100g/min; $p = 0.0015$), maintaining increased levels in post-tDCS (176.86 ± 28.58 μmol/100g/min).

Conclusions: tDCS has immediate effects on neuronal excitability, as measured by increased cerebral blood supply and oxygen consumption supporting increased neuronal firing. These findings provide a standard range of CBF and $CMRO_2$ changes due to tDCS in healthy adults that may be incorporated in clinical studies to evaluate its therapeutic potential.

1. Introduction

tDCS modulates cortical excitability of targeted brain regions by applying weak electrical currents to alter transcranial polarization (Bikson et al., 2016; Dedoncker et al., 2021; Nitsche et al., 2008). It has been used as an alternative treatment in a wide range of clinical settings for the management of neurological and psychiatric conditions. Prior studies have demonstrated clinical and cognitive improvement using tDCS in conditions including attention deficit hyperactivity disorder (ADHD) (Breitling et al., 2016; Prehn-Kristensen et al., 2014), stroke (Khedr et al., 2013; O'Shea et al., 2014), Parkinson's Disease (PD) (Doruk et al., 2014; Ishikuro et al., 2018; Pereira et al., 2013), multiple sclerosis (MS) (Chalah et al., 2017; Charvet et al., 2018a; Charvet et al., 2018b) and others (Fiori et al., 2013; Fregni et al., 2021; Fregni et al., 2020; Mrakic-Sposta et al., 2008; San-Juan et al., 2017; Soler et al., 2010). Despite its positive clinical findings as a treatment approach, establishing a frame of reference for the biophysiological underpinnings of tDCS in healthy subjects remains of great importance.

* Corresponding author.
E-mail address: yulin.ge@nyulangone.org (Y. Ge).

https://doi.org/10.1016/j.brainres.2022.148097
Received 23 June 2022; Received in revised form 6 September 2022; Accepted 16 September 2022
Available online 20 September 2022

Recent developments in tDCS applied with simultaneous MRI (or tDCS-MRI) can provide insights on the stimulation-induced effects and more directly characterize the underlying neuronal response by maximizing its stimulation effects, which can fill the gap of knowledge regarding whether and how externally applied tDCS modifies neuronal activity and cerebral blood flow (CBF).

Prior studies have reported that tDCS increases CBF in both local areas targeted by the stimulation and remote areas (Jamil et al., 2020; Merzagora et al., 2010; Zheng et al., 2011), which is likely due to the neurovascular coupling mechanism indicated on blood oxygenation level dependent (BOLD) functional MRI (Ogawa et al., 1990). In addition, cerebral metabolic rate of oxygen ($CMRO_2$) provides a direct and objective measure of neural activation. By measuring global $CMRO_2$ change from pre- to during-tDCS, one can quantify the amount of neuronal response or neuronal reactivity (NR). In this study, we characterized the simultaneous $CMRO_2$ changes due to tDCS using a T2-relaxation-under-spin-tagging (TRUST) (Lu and Ge, 2008) MRI technique in healthy adults. Global $CMRO_2$ was quantified using the venous blood oxygenation (Yv) as well as CBF obtained via phase contrast imaging (as previously described by Xu et al. (2009)). We hypothesized that CBF and $CMRO_2$ would increase with tDCS, representing an increase in neuronal activity. Investigating both simultaneous and immediate post-tDCS effects using quantitative oxygen metabolic measures makes this study, to the best of our knowledge, the first to provide a standard of healthy neuronal reaction to tDCS. Comparisons with this reference frame can therefore be used to investigate the potential therapeutic effects of tDCS on clinical populations by observing changes in global neuronal activity due to treatment.

2. Methods

This study was completed with IRB approval from NYU Langone Health. Participants were recruited through the NYU Langone Health Division of MS in the department of neurology as part of a larger clinical study. Imaging was completed at the NYU Langone Health Center for Biomedical Imaging in the department of radiology.

2.1. Participants

Thirty healthy participants were recruited to complete the simultaneous tDCS-MRI scan protocol in a single visit. All participants were screened and excluded if there was a history of head injury, neurological disease, presence of implanted metal in the body or medical device (e.g., deep brain stimulator, vagus nerve stimulator) and any contraindications for MRI (e.g., pregnancy, extreme claustrophobia, irremovable piercings, metallic-based tattoos) or tDCS (e.g., skin disorders or sensitive skin under the electrode area). Three subjects were excluded from further analysis due to partial data; two subjects were excluded due to incidental finding of unexpected brain structural pathologies and two more subjects due to suboptimal image quality. The final group size, used for this report, was therefore of 23 healthy subjects (HC; age = 35.6 ± 15.0 years old, 10 males).

2.2. Experimental design and data acquisition

Stimulation was delivered using a MRI-compatible tDCS device (1x1 tDCS Model 1300A Low-Intensity Stimulator, Soterix Medical Inc.) and via two MRI-compatible conductive rubber electrodes inserted in a saline-soaked sponge (5 × 5 cm), placed over the frontal lobe with the anode on the left dorsolateral prefrontal cortex (F3, DLPFC) and the cathode over the right DLPFC (F4; Fig. 1A), per protocol for the larger clinical trial studying the effects of tDCS on fatigue and cognitive functioning in participants with MS. The current intensity was set at 2.0 mA and was manually ramped-up and ramped-down in about 30 seconds.

MRI images were acquired in a 3 T MRI (Prisma, Siemens) fitted with a 64-channels head coil. The experimental procedure consisted of simultaneous tDCS inside the MRI and was divided in three main phases. A 'pre-tDCS' phase, lasting about 20–30 minutes, during which no stimulation was given to the subject and conventional FLAIR was acquired for lesion detection and a time of flight (TOF) was acquired to be used as a MR angiographic reference image to place phase-contrast (PC) MRI. It was followed by a 'during-tDCS' phase lasting 15 minutes, during which subjects received a tDCS at 2.0 mA and finally a 'post-tDCS' phase lasting 15–20 minutes during which the tDCS device was turned off and no stimulation was given to the subject. The scanning procedure is represented in Fig. 1B. In each phase, the same PC-MRI for CBF and TRUST sequence for Yv measurement were performed and repeated in order to address the expected physiological effects from the stimulation. To allow the stimulation to ramp-up and reach the target current intensity, brain structural data was acquired at the beginning of the 'during-tDCS' phase using 3D T1 MPRAGE.

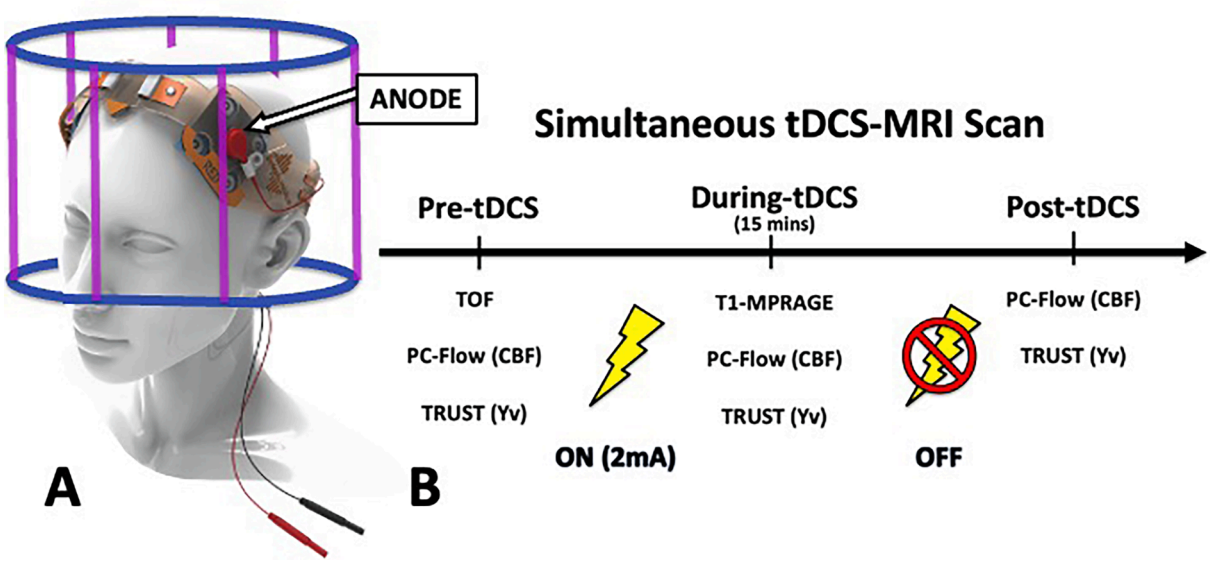

Fig. 1. (A) Left anodal dorsolateral prefrontal cortex electrode montage representation. (B) experimental design during which MRI image acquisition was obtained in three sessions: before the stimulation (pre-tDCS), during 15 minutes 2.0 mA stimulation (during-tDCS) and right after turning off the stimulation (post-tDCS).

Arterial blood flow was imaged using axial PC-MRI sequence (TR = 25 ms, TE = 8 ms, slice thickness = 5 mm, flip angle = 15°, FoV =0.5x0.5x5mm) which encodes the velocity of the flowing spins in the main neck arteries, above the carotid bifurcation. The positioning of the PC scan was based on the TOF angiogram and the imaging slice was perpendicular to each individual neck artery, bilateral carotid arteries (ICAs) and bilateral vertebral arteries (VAs), with respect to the blood flow to ensure flow quantification accuracy. The acquisition time of each PC-MRI was 10 seconds. Velocity encoding (VENC) parameter was 60 cm/s for arterial flow, which is in the range of what commonly used (60–100 cm/s) (Debbich et al., 2020; Mendieta et al., 2020; Rivera-Rivera et al., 2021; Shin and Shin, 2020). The resulting phase and magnitude PC-MRI images therefore represent a single timepoint measurement from each of the three sessions (pre-, during- and post-tDCS).

TRUST MRI (Lu and Ge, 2008) was performed in a transverse plane parallel to the anterio-posterior commissure line and going through the lower superior sagittal sinus (just above the level of confluence of sinuses) for a global estimation of oxygen consumption. For each scan, the sequence begins with a presaturation RF pulse to suppress the static tissue signal (to improve the signal-to-noise ratio) and it is followed by a labeling (or control) RF pulse to magnetically label the venous blood. By performing a subtraction of labeled and control images, only flowing signal remains in the difference image reflecting pure venous blood. The T2-relaxation time of the blood is estimated by repeating the label/control pairs but with increasing T2-weighting. To minimize the effect of blood outflow on the estimation, a nonselective T2-preparation pulse train is employed for T2-weighting, the duration of which is denoted effective echo time (eTE), instead of the typical multispin-echo acquisition. Therefore, a complete TRUST MRI sequence includes both labeled and control scans acquired at different eTEs for different T2-weightings. The specific imaging parameters of TRUST were as follows: TA = 87 seconds, TR/TE/TI = 3,000/19/1,200 ms, repetition = 4, FoV = 230 mm × 230 mm, matrix = 64 × 64, single-shot echo planar imaging, slice thickness = 5 mm, four eTEs: 0, 40, 80, and 160 ms, corresponding to 0, 4, 8, and 16 refocusing pulses with an interval (τCPMG) of 10 ms in the T2-preparation.

2.3. MRI data analysis

All data were processed offline using in-house-written MATLAB (Mathworks, Natick, MA, USA) scripts. After the MRI data was acquired, structural images were analyzed using SPM12 (Wellcome Trust Center for Neuroimaging, Institute of Neurology, London UK) to extract gray matter (GM), white matter (WM) and cerebrospinal fluid (CSF) volumes (mL) needed to calculate the subject's brain parenchymal volume (BPV). PC-MRI images, obtained by placing the imaging slices on the TOF image perpendicular to the blood flow (Fig. 2A), were then used to quantify each artery's CBF. This was extracted by manually drawing a region of interest (ROI) around each individual artery's cross-section on the axial magnitude phase contrast image (Fig. 2B). The ROI was then transposed to the corresponding phase contrast image and the average pixel intensity was used to calculate the average velocity of blood for the specific vessel. This allowed for a separate quantification of blood flowing through the left and right interior carotid artery (LICA and RICA) as well as left and right vertebral artery (LVA and RVA). For group comparison, the obtained CBF values were normalized using the individual-specific BPV (Fig. 2C) using equation 1.

$$CBF = \frac{BF}{\rho \times BPV} \times 100$$

where CBF is the normalized blood flow; BF is the total blood flow output from the PC-MRI sequence; ρ is the brain tissue density (1.06 g/mL) and BPV is the brain parenchymal volumes obtained from T1 MPARAGE segmentation.

The details of data processing procedures for TRUST MRI and estimation of $CMRO_2$ were described previously (Lu and Ge, 2008; Xu et al., 2009). In short, the TRUST data consist of labeled and control images acquired at the lower part of the superior sagittal sinus (Fig. 3A). Each image type is acquired with four different eTEs. The preprocessing includes pairwise subtraction to ensure that only blood signal draining

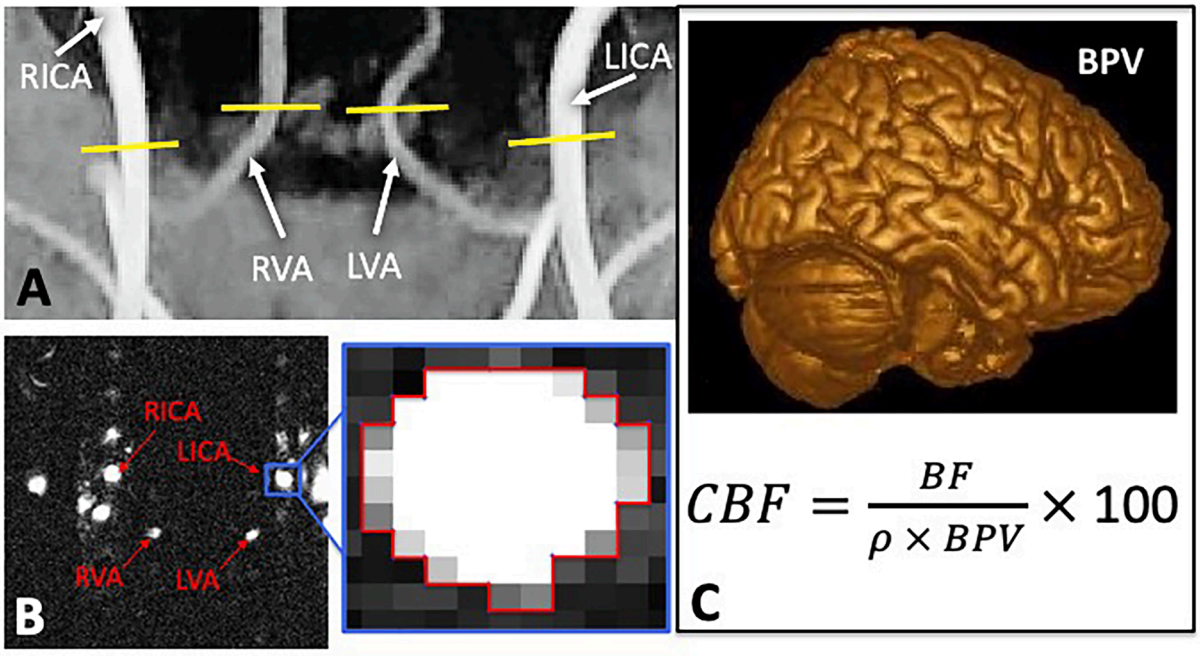

Fig. 2. (A) Coronal view time of flight (TOF) image of the four main brain feeding arteries in the neck used to place the phase contrast (PC) imaging slices of each individual artery (B) Axial phase contrast-MRI magnitude image used to draw regions of interest (ROIs) around cross-sections of the 4 brain feeding arteries: left and right internal carotid arteries (LICA and RICA); left and right vertebral arteries (LVA and RVA). This allowed for extraction of vessel-specific blood flux and total blood flux (ml/min). (C) Equation used to calculate the global cerebral blood flow (CBF), using the total blood flow from both ICAs and VAs, measured by PC-MRI (BF), brain tissue density (ρ = 1.06 g/mL) and finally the brain parenchymal volume (BPV), represented above.

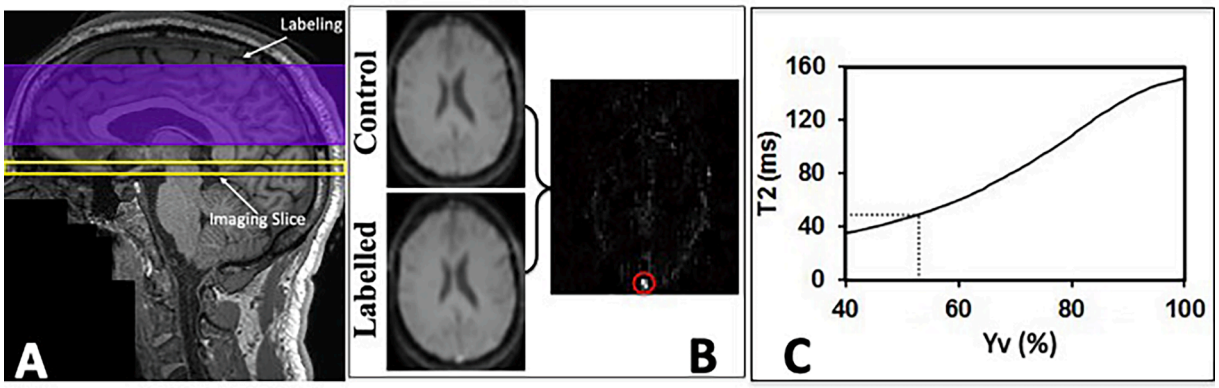

Fig. 3. (A) Positioning of imaging and labeling slice for the T2-Relaxation-Under-Spin-Tagging (TRUST) sequence on a representative T1 image. (B) Obtained axial control and labelled magnitude images (left) using the TRUST sequence and linear subtraction of the two (labelled-control; right) used to draw and ROI (red circle) to extract corresponding T2 values of the venous blood at the inferior part of the superior sagittal sinus. (C) Calibration correlation curve of T2 signal used to estimate corresponding venous blood oxygenation (Yv).

into the superior sagittal sinus is shown and quantified (Fig. 3B), thus excluding the possibility of measuring other tissues in the venous sinus, such as CSF partial volume, dura matter, or granular tissue. The signals from different eTEs were fitted to obtain CPMG (Carr-Purcell-Meiboom-Gill) T2 of the venous blood. Based on a well-established correlation between blood T2-relaxation time and blood oxygen saturation (Golay et al., 2001; Wright et al., 1991; Zhao et al., 2007), Yv is then converted from the venous blood T2 using this calibration correlation (Fig. 3C). Using the data obtained for Yv and CBF, the index $CMRO_2$ was then calculated. This measure combines the arterial blood supplied to the brain and the magnitude of unused oxygen drained into the venous blood to calculate the global neuronal activity. For this study, $CMRO_2$ is an index of the amount of O_2 molecules consumed per unit mass tissue per unit time calculated using equation 2, as previously reported by Xu et al. (2009).

$$CMRO_2 = CBF \times (Y_a - Y_v) \times C_a \quad [2]$$

where CBF is the normalized cerebral blood flow measured in mL/100 g/min; Y_a and Y_v are the arterial and venous blood oxygenation in % and C_a is a constant representing the amount of oxygen-carrying molecules per unit volume of blood. In males $C_a = 8.562273$ and in females $C_a = 8.154545$(Guyton and Hall, 2006).

2.4. Statistical analysis

A paired *t*-test was then used to assess the hypothesized differences of this physiological factors between combinations of pre-, during- and post-tDCS. An independent *t*-test was used to investigate sex-related effects on tDCS efficacy, comparing male and female subjects' data, and a linear correlation analysis was utilized to address the potential effects of age on the results. Level of statistical significance was set at 0.05. Analysis and graphical representation were carried out using Matlab 2019a (The Mathworks Inc., Natick, Massachusetts USA) and GraphPad Prism version 9.0.0 for Mac (GraphPad Software, San Diego, California USA).

3. Results

As observable in Fig. 4A, the global CBF, from four feeding arteries of the brain, measured during the stimulation (57.10 ± 8.33 mL/100g/min) was significantly greater compared to what measured in pre-tDCS (53.67 ± 7.75 mL/100g/min; $p < 0.0001$) in these healthy adults. However, no significant change was observed when comparing during- and post-tDCS (56.79 ± 8.70 mL/100g/min; $p = 0.7475$), indicating that CBF remains significantly ($p = 0.0009$) greater than pre-tDCS even in post-tDCS. The level of oxygenation measured before applying the stimulation (60.71 ± 4.12 %) did not significantly differ ($p > 0.005$)

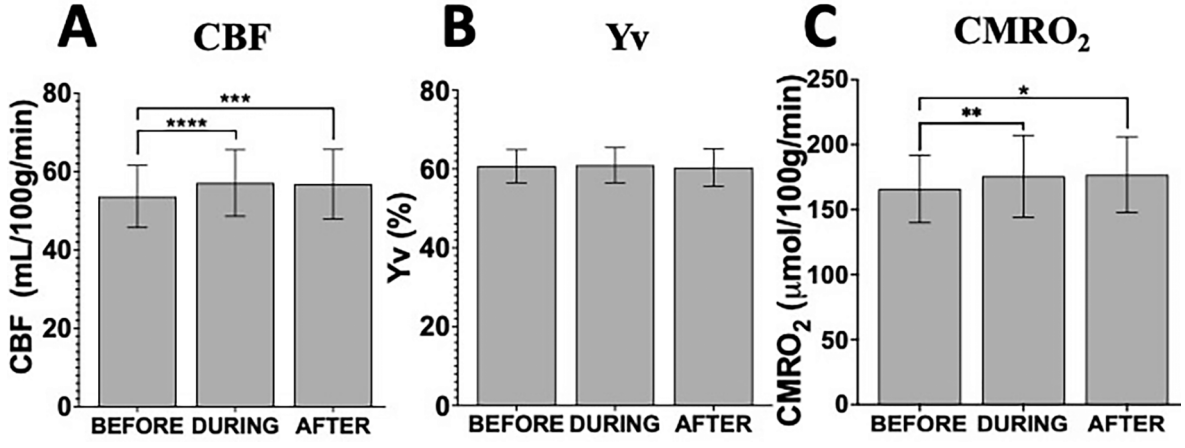

Fig. 4. MRI data measured at three timepoints with respect to tDCS application (before, during and after) for cerebral blood flow (CBF; A), venous blood oxygenation (Yv; B) and calculated cerebral metabolic rate of oxygen ($CMRO_2$; C). Note that the increased oxygen supply through increased CBF due to tDCS does not lead to increased oxygen output in the venous blood (Yv), which suggests that the excessive oxygen supply is readily compensated by increased neuronal activity ($CMRO_2$) from stimulation. Also note that the increased neuronal activity persists after tDCS.

from what measured during-tDCS (60.96 ± 4.37 %) nor from post-tDCS (60.39 ± 4.66 %), as shown in Fig. 4B. $CMRO_2$ represents an index of how well the neuronal and hemodynamic properties are interlocked. We observed that the level of oxygen consumption, measured by $CMRO_2$, increased from 165.84 ± 25.32 μmol/100g/min (pre-tDCS) to 175.68 ± 30.78 μmol/100g/min during the stimulation ($p = 0.0015$). As observed in the global CBF analysis, $CMRO_2$ levels also remain relatively constant post-tDCS (176.86 ± 28.58 μmol/100g/min) when compared to during-tDCS ($p > 0.05$; Fig. 4C). Measurements at all three timepoints and corresponding p-values are summarized in Table 1.

Analyses were repeated to test for the contribution of factors such as: sex, age and brain volumes. A sex-related effect was only observed in relation to global CBF but consistently in pre- ($p = 0.042$), during-($p = 0.045$) and post-tDCS ($p = 0.037$). It should be also noted that the percentage changes recorded from pre- to during-tDCS did not seem to be different in males compared to the response observed in females for neither one of the three biophysiological parameters (CBF, Yv, $CMRO_2$). Despite such results on sex-related effects, it must be noted that the group size in this study is too small to support a definite conclusion.

Linear regression analysis was also adopted to investigate possible age-related effects on tDCS response (during-tDCS), expressed as percentage change from what measured in pre-tDCS. We observed no significant correlations ($p > 0.05$) between age and percentage change due to tDCS except for a positive correlation with CBF percentage change as response to tDCS (during-tDCS). However, this might be due to the sample size being too small, and the age range too narrow, to truly appreciate any age-related influences.

4. Discussion

Using a simultaneous tDCS-MRI protocol in healthy adults, we applied left anodal DLPFC tDCS to measure real-time and persisting changes of blood flow and neuronal oxygen metabolic response. At the group level, we found that 15 minutes of tDCS application results in an immediate increase in neuronal activity, measured by global $CMRO_2$, and supported by a comparable increase in whole brain CBF. More importantly, these effects were observed to persist immediately after the stimulation period.

These results elucidate the mechanisms of neuronal responses to tDCS, specifically oxygen metabolism changes, simultaneously (during-tDCS) and immediately after (post-tDCS) for lingering effects. Furthermore, our findings provide potential references for future clinical studies to evaluate and identify patients who will be more likely to show a response to tDCS treatments.

$CMRO_2$ provides a direct *in-vivo* measure of neuronal cells' metabolic activity and vitality and therefore is an ideal tool to noninvasively assess neuronal reactivity (NR) to tDCS. NR can be assessed by quantifying the percent change of $CMRO_2$ from baseline and represents the total potential neuronal response which can be used to predict tDCS clinical outcome (i.e., responders *vs* non-responders) on which virtually no research has been done. Developing an *in-vivo* method to objectively monitor the tDCS-induced bioeffects is important to guide further tDCS interventions in patients, particularly in choosing patients who have higher neuroplastic potential or neuronal response to tDCS and therefore could benefit more from tDCS treatment. Although tDCS introduces electrical currents in the MRI environment, which might distort the magnetic field, our imaging measurements were far from the stimulation site: PC-MRI imaging slice placed at the neck and TRUST imaging slice in the lower superior sagittal sinus. Furthermore, these sequences are less susceptible to field inhomogeneities compared to other ones (e.g. gradient echo).

As a result of the increase in neuronal activity and oxygen consumption during-tDCS, a decrease in venous oxygen saturation, or Yv, could be expected. However, no change in Yv levels pre- and during-tDCS were observed in this study, suggesting that the increased oxygen delivery, caused by increased CBF, might be consumed by increased cortical activation, or oxygen consumption, leading to the reported balanced Yv. In this study we found that tDCS resulted in an immediate 6.5 % increase in whole brain CBF via the four main neck-feeding arteries and 5.9 % global $CMRO_2$ increase compared to pre-tDCS measurements. This contrasts with the 1 ~ 2 % BOLD signal changes seen in region-specific task-related fMRI studies, suggesting the externally applied tDCS may cause larger scale neuronal response and may be more robust to evaluate neuronal activity. Simultaneous $CMRO_2$ measure using tDCS-MRI may therefore provide a good global marker of neuronal response in patients through the change in oxygen consumed by the neurons due to tDCS. Fig. 5 summarizes the tDCS-related changes in CBF, Yv and $CMRO_2$ reported in this study. Moreover, our findings are consistent with previous MRI studies reporting tDCS-related increase in brain activity (Chib et al., 2013; Liebrand et al., 2020; Meyer et al., 2019; Sotnikova et al., 2017), recently reviewed in Chang et al. (2021). However, the bio-physiological mechanisms of tDCS might be more complex, with different levels of oxygen metabolism change (Yoon et al., 2014).

As seen in task-based fMRI studies, in which increased neuronal activity is associated with increased regional CBF due to neurovascular coupling, we found global increase in CBF observed during-tDCS compared to pre-tDCS, which is also likely due to the provoked neuronal activity. Even though the current flow is delivered locally, it can propagate diffusely to remote cortical regions with diffused global effects (Bikson and Datta, 2012; Datta et al., 2013). Recent fMRI studies have also shown that anodal left DLPFC tDCS causes a general increase in brain perfusion during the stimulation but with greater changes observed in brain structures that were anatomically and functionally closer to the stimulation site (Stagg et al., 2013; Zheng et al., 2011). The persisting CBF increase after the stimulation period suggests that tDCS not only effectively increases the brain's vascular supply, but also that its effects linger after the stimulation is stopped. Similar hemodynamic changes have been previously reported (Jamil et al., 2020; Merzagora et al., 2010; Zheng et al., 2011), and suggest that the increase in neuronal activity due to tDCS is strongly linked to neurovascular coupling. Further investigation is needed to quantitatively describe the separate contributions of vascular and neuronal oxygen metabolism changes in response to tDCS.

As with CBF, $CMRO_2$ levels increased with tDCS and remained increased after the stimulation period. These findings support the potential presence of lingering tDCS effects that persist for a period of time after the stimulation is ended. While the duration of such effect is not known, both human (Agboada et al., 2019; Fricke et al., 2011; Monte-Silva et al., 2013; Mosayebi Samani et al., 2019) and preclinical (Liu

Table 1
Changes due to tDCS in CBF, Yv and $CMRO_2$.

Parameter	PRE-tDCS (mean ± SD)	DUR-tDCS (mean ± SD)	POST-tDCS (mean ± SD)	p-value (paired t-test)		
				PRE vs DUR	DUR vs POST	PRE vs POST
Global CBF (mL/100g/min)	53.67 ± 7.75	57.10 ± 8.33	56.79 ± 8.70	<0.0001****	0.7475	0.0009***
Yv (%)	60.71 ± 4.12	60.96 ± 4.37	60.39 ± 4.66	0.6698	0.4887	0.7167
$CMRO_2$ (μ mol/100g/min)	165.84 ± 25.32	175.68 ± 30.78	176.86 ± 28.58	0.0015**	0.7971	0.0150*

Notes: Comprehensive table of measurements for global cerebral blood flow (CBF), venous blood oxygenation (Yv) and calculated cerebral metabolic rate of oxygen ($CMRO_2$). Interestingly, the elevated levels of CBF and $CMRO_2$ due to tDCS persist even after the stimulation (post-tDCS).

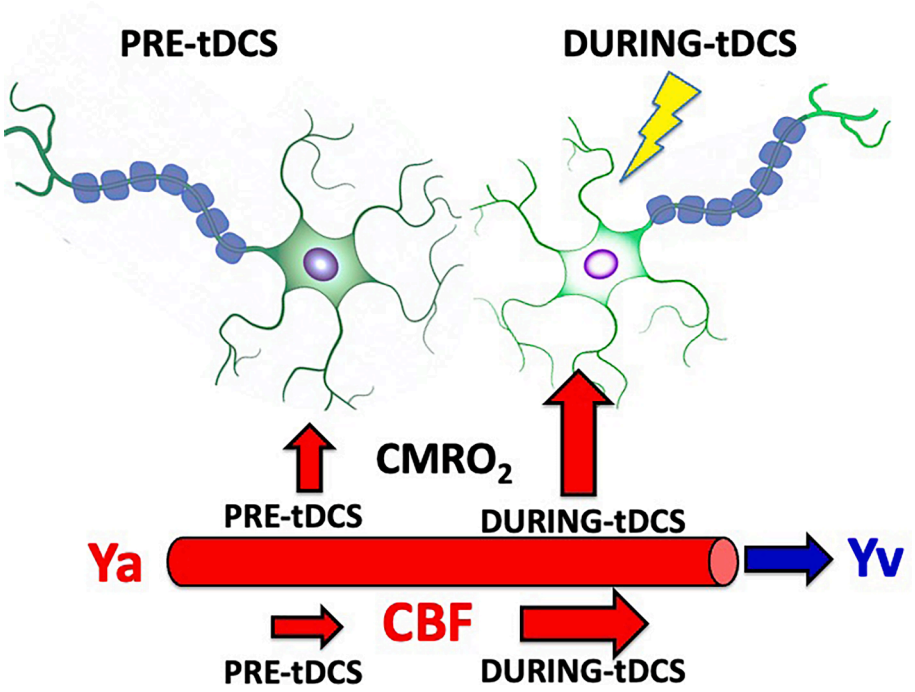

Fig. 5. Schematic diagram shows representative levels of oxygenated (Ya) cerebral blood flow (CBF), venous blood oxygenation (Yv) and calculated cerebral metabolic rate of oxygen ($CMRO_2$) before and during tDCS. Note that during the stimulation, the increase in oxygen input, as consequence of increase CBF (6.5%), almost exactly corresponds to the increased neuronal activity or increased $CMRO_2$, (5.9%) due to tDCS. Consequently, leaving the similar levels of oxygen output in the Yv.

et al., 2019; Zhao et al., 2020) studies have suggested that this may persist for hours after the stimulation is turned off. Furthermore, tDCS has a known cumulative effect through repeated sessions (e.g. daily for a period of weeks or months) with the goal of altering the brain's neuronal activity and functional connectivity (Ficek et al., 2018; Mondino et al., 2018; Wu et al., 2019). However, the interval window between consecutive tDCS sessions has been observed to considerably influence the stimulation's effects (Agboada et al., 2020; Monte-Silva et al., 2013) and an optimal threshold has yet to be completely identified. Therefore, further definition of its persisting effects may directly inform its future clinical application.

Although studies have previously reported age-related influences on tDCS-effects (Alisch et al., 2021; Antonenko et al., 2018; Woods et al., 2019), in our study no such characteristic was observed. However, this could be due to the small sample size and narrow age range of our study, which does not allow for confident age-related effects analysis. Similarly, although the sex-related effects observed in this study are in line with previous reports of a greater CBF observed in female compared to male subjects (Aanerud et al., 2017; Alisch et al., 2021), further studies, with larger group sizes, are warranted to confirm any sex-related effects on tDCS neuromodulation.

There are some limitations to our study besides the relatively small sample size and narrow, younger age range of our participants. While we characterized global tDCS response, it is not known whether the current findings are specific to the tDCS parameters of intensity (Ammann et al., 2017; Chew et al., 2015; Dedoncker et al., 2016; Dissanayaka et al., 2017; Hoy et al., 2013; Iyer et al., 2005; Jamil et al., 2017; Nitsche and Paulus, 2000; Teo et al., 2011), montage (Penolazzi et al., 2013), or duration (Hassanzahraee et al., 2020; Nitsche and Paulus, 2000). In addition, a control or sham-tDCS group could have strengthen the quality of our results. However, ours is a mechanistic real-time tDCS study, focusing on the within subject biophysiological changes due to tDCS and not on the clinical outcomes of tDCS treatment. Therefore, we do not think that a sham-tDCS control group would have significantly affected the conclusions presented in this work. A regional CBF analysis may provide a fuller understanding of the compensating inner mechanisms of the cerebrovascular response. Further research and technology development providing regional information will contribute to better understating the individual region-specific response to tDCS.

This study adds to the growing literature supporting tDCS-induced cortical excitability and increase in CBF that can be quantified with the proposed $CMRO_2$ and phase contrast MRI approaches. These global real-time effects are often missed, or hard to appreciate, in typical fMRI paradigms. The characterization of these effects in a sample of healthy adults can provide a reference for comparison in future patient studies.

Declaration of Competing Interest

Soterix Medical Inc. provided the tDCS equipment used for research use. The City University of New York holds patents on brain stimulation with MB as inventor. The City University of New York holds patents on brain stimulation with AD as inventor. AD is an employee of Soterix Medical Inc. AD has equity in Soterix Medical Inc. MB has equity in Soterix Medical Inc. MB consults, received grants, assigned inventions, and/or serves on the SAB of SafeToddles, Boston Scientific, GlaxoSmithKline, Biovisics, Mecta, Lumenis, Halo Neuroscience, Google-X, i-Lumen, Humm, Allergan (Abbvie), Apple.

Data availability

Data will be made available on request.

Acknowledgments

Funding.

LC is supported by grants NIH: R01 NS112996, R21 HD094424, US Department of Defense: W81XWH-17–1-0320, VA Healthcare: GRANT13010404, National MS Society: RG-1803–30492, RFA-2104–37483, and NIDA-NIH: R21 DA055427. MB is supported by grants from Harold Shames and the National Institutes of Health: NIH-NIDA

UG3DA048502, NIH-NIGMS T34GM137858, NIH-NINDS 1R01NS112996, NIH-NINDS 1R01NS101362, NIH-NIMH 1R01MH111896, and NIH-NINDS 1R01NS095123. AD is supported by grants from: NIH-NIDA 75N95020C00024, DoD-DARPA: W912CG21C0014, ED: 91990021C0032. YG is supported by the National Institute of Health (NIH) under award numbers: R21 HD094424, RF NS110041, R01 NS108491, R01 AG077422, and R13 AG067684. GP is supported by grants from DOD US: W81XWH-22-1-0812, National MS Society: RFA-2104–37483, and NIDA-NIH: R21 DA055427.

References

Aanerud, J., et al., 2017. Sex differences of human cortical blood flow and energy metabolism. J. Cereb. Blood Flow Metab. 37, 2433–2440.
Agboada, D., et al., 2019. Expanding the parameter space of anodal transcranial direct current stimulation of the primary motor cortex. Sci. Rep. 9, 18185.
Agboada, D., et al., 2020. Induction of long-term potentiation-like plasticity in the primary motor cortex with repeated anodal transcranial direct current stimulation - Better effects with intensified protocols? Brain Stimul. 13, 987–997.
Alisch, J.S.R., et al., 2021. Sex and age-related differences in cerebral blood flow investigated using pseudo-continuous arterial spin labeling magnetic resonance imaging. Aging (Albany NY) 13, 4911–4925.
Ammann, C., Lindquist, M.A., Celnik, P.A., 2017. Response variability of different anodal transcranial direct current stimulation intensities across multiple sessions. Brain Stimul. 10, 757–763.
Antonenko, D., et al., 2018. Age-dependent effects of brain stimulation on network centrality. Neuroimage 176, 71–82.
Bikson, M., et al., 2016. Safety of Transcranial Direct Current Stimulation: Evidence Based Update 2016. Brain Stimul. 9, 641–661.
Bikson, M., Datta, A., 2012. Guidelines for precise and accurate computational models of tDCS. Brain Stimul. 5, 430–431.
Breitling, C., et al., 2016. Improving Interference Control in ADHD Patients with Transcranial Direct Current Stimulation (tDCS). Front. Cell. Neurosci. 10, 72.
Chalah, M.A., et al., 2017. Effects of left DLPFC versus right PPC tDCS on multiple sclerosis fatigue. J. Neurol. Sci. 372, 131–137.
Chang, K.-Y., et al., 2021. tDCS and Functional Connectivity. In: Transcranial Direct Current Stimulation in Neuropsychiatric Disorders: Clinical Principles and Management. Vol., A.R. Brunoni, M.A. Nitsche, C.K. Loo, ed.ˆeds. Springer International Publishing, Cham, pp. 159-172.
Charvet, L., et al., 2018a. Remotely supervised transcranial direct current stimulation increases the benefit of at-home cognitive training in multiple sclerosis. Neuromodulation 21, 383–389.
Charvet, L.E., et al., 2018b. Remotely supervised transcranial direct current stimulation for the treatment of fatigue in multiple sclerosis: Results from a randomized, sham-controlled trial. Mult. Scler. 24, 1760–1769.
Chew, T., Ho, K.A., Loo, C.K., 2015. Inter- and intra-individual variability in response to transcranial direct current stimulation (tDCS) at varying current intensities. Brain Stimul. 8, 1130–1137.
Chib, V.S., et al., 2013. Noninvasive remote activation of the ventral midbrain by transcranial direct current stimulation of prefrontal cortex. Transl. Psychiatry 3, e268.
Datta, A., et al., 2013. Validation of finite element model of transcranial electrical stimulation using scalp potentials: implications for clinical dose. J. Neural Eng. 10, 036018.
Debbich, A., et al., 2020. A spatiotemporal exploration and 3D modeling of blood flow in healthy carotid artery bifurcation from two modalities: ultrasound-doppler and phase contrast MRI. Comput. Biol. Med. 118, 103644.
Dedoncker, J., et al., 2016. A systematic review and meta-analysis of the effects of transcranial direct current stimulation (tDCS) over the dorsolateral prefrontal cortex in healthy and neuropsychiatric samples: influence of stimulation parameters. Brain Stimul. 9, 501–517.
Dedoncker, J., et al., 2021. Combined transcranial direct current stimulation and psychological interventions: State of the art and promising perspectives for clinical psychology. Biol. Psychol. 158, 107991.
Dissanayaka, T., et al., 2017. Does transcranial electrical stimulation enhance corticospinal excitability of the motor cortex in healthy individuals? A systematic review and meta-analysis. Eur. J. Neurosci. 46, 1968–1990.
Doruk, D., et al., 2014. Effects of tDCS on executive function in Parkinson's disease. Neurosci. Lett. 582, 27–31.
Ficek, B.N., et al., 2018. The effect of tDCS on functional connectivity in primary progressive aphasia. Neuroimage Clin. 19, 703–715.
Fiori, V., et al., 2013. tDCS stimulation segregates words in the brain: evidence from aphasia. Front. Hum. Neurosci. 7, 269.
Fregni, F., et al., 2021. Evidence-based guidelines and secondary meta-analysis for the use of transcranial direct current stimulation in neurological and psychiatric disorders. Int. J. Neuropsychopharmacol. 24, 256–313.
Fregni, F., El-Hagrassy, M.M., Pacheco-Barrios, K., Carvalho, S., Leite, J., Simis, M., Brunelin, J., Nakamura-Palacios, E.M., Marangolo, P., Venkatasubramanian, G., San-Juan, D., 2020. Evidence-based guidelines and secondary meta-analysis for the use of transcranial direct current stimulation (tDCS) in neurological and psychiatric disorders. Int. J. Neuropsychopharmacol.
Fricke, K., et al., 2011. Time course of the induction of homeostatic plasticity generated by repeated transcranial direct current stimulation of the human motor cortex. J. Neurophysiol. 105, 1141–1149.
Golay, X., et al., 2001. Time-resolved contrast-enhanced carotid MR angiography using sensitivity encoding (SENSE). AJNR Am. J. Neuroradiol. 22, 1615–1619.
Guyton, A.C., Hall, J.E., 2006. Textbook of medical physiology. Elsevier Saunders, Philadelphia, pp. 859–863.
Hassanzahraee, M., et al., 2020. Determination of anodal tDCS duration threshold for reversal of corticospinal excitability: an investigation for induction of counter-regulatory mechanisms. Brain Stimul. 13, 832–839.
Hoy, K.E., et al., 2013. Testing the limits: Investigating the effect of tDCS dose on working memory enhancement in healthy controls. Neuropsychologia 51, 1777–1784.
Ishikuro, K., et al., 2018. Effects of transcranial direct current stimulation (tDCS) over the frontal polar area on motor and executive functions in parkinson's disease. A Pilot Study. Front Aging Neurosci. 10, 231.
Iyer, M.B., et al., 2005. Safety and cognitive effect of frontal DC brain polarization in healthy individuals. Neurology 64, 872–875.
Jamil, A., et al., 2017. Systematic evaluation of the impact of stimulation intensity on neuroplastic after-effects induced by transcranial direct current stimulation. J. Physiol. 595, 1273–1288.
Jamil, A., et al., 2020. Current intensity- and polarity-specific online and aftereffects of transcranial direct current stimulation: an fMRI study. Hum. Brain Mapp. 41, 1644–1666.
Khedr, E.M., et al., 2013. Effect of anodal versus cathodal transcranial direct current stimulation on stroke rehabilitation: a pilot randomized controlled trial. Neurorehabil Neural Repair. 27, 592–601.
Liebrand, M., et al., 2020. Beneficial effects of cerebellar tDCS on motor learning are associated with altered putamen-cerebellar connectivity: a simultaneous tDCS-fMRI study. Neuroimage 223, 117363.
Liu, H.H., et al., 2019. Neuromodulatory effects of transcranial direct current stimulation on motor excitability in rats. Neural Plast. 2019, 4252943.
Lu, H., Ge, Y., 2008. Quantitative evaluation of oxygenation in venous vessels using T2-Relaxation-Under-Spin-Tagging MRI. Magn. Reson. Med. 60, 357–363.
Mendieta, J.B., et al., 2020. The importance of blood rheology in patient-specific computational fluid dynamics simulation of stenotic carotid arteries. Biomech. Model. Mechanobiol. 19, 1477–1490.
Merzagora, A.C., et al., 2010. Prefrontal hemodynamic changes produced by anodal direct current stimulation. Neuroimage 49, 2304–2310.
Meyer, B., et al., 2019. Increased neural activity in mesostriatal regions after prefrontal transcranial direct current stimulation and l-DOPA administration. J. Neurosci. 39, 5326–5335.
Mondino, M., et al., 2018. Effects of repeated transcranial direct current stimulation on smoking, craving and brain reactivity to smoking cues. Sci. Rep. 8, 8724.
Monte-Silva, K., et al., 2013. Induction of late LTP-like plasticity in the human motor cortex by repeated non-invasive brain stimulation. Brain Stimul. 6, 424–432.
Mosayebi Samani, M., et al., 2019. Titrating the neuroplastic effects of cathodal transcranial direct current stimulation (tDCS) over the primary motor cortex. Cortex 119, 350–361.
Mrakic-Sposta, S., et al., 2008. Transcranial direct current stimulation in two patients with Tourette syndrome. Mov. Disord. 23, 2259–2261.
Nitsche, M.A., et al., 2008. Transcranial direct current stimulation: State of the art 2008. Brain Stimul. 1, 206–223.
Nitsche, M.A., Paulus, W., 2000. Excitability changes induced in the human motor cortex by weak transcranial direct current stimulation. J. Physiol. 527 (Pt 3), 633–639.
Ogawa, S., et al., 1990. Brain magnetic resonance imaging with contrast dependent on blood oxygenation. Proc. Natl. Acad. Sci. U.S.A. 87, 9868–9872.
O'Shea, J., et al., 2014. Predicting behavioural response to TDCS in chronic motor stroke. Neuroimage 85 (Pt 3), 924–933.
Penolazzi, B., Pastore, M., Mondini, S., 2013. Electrode montage dependent effects of transcranial direct current stimulation on semantic fluency. Behav. Brain Res. 248, 129–135.
Pereira, J.B., et al., 2013. Modulation of verbal fluency networks by transcranial direct current stimulation (tDCS) in Parkinson's disease. Brain Stimul. 6, 16–24.
Prehn-Kristensen, A., et al., 2014. Transcranial oscillatory direct current stimulation during sleep improves declarative memory consolidation in children with attention-deficit/hyperactivity disorder to a level comparable to healthy controls. Brain Stimul. 7, 793–799.
Rivera-Rivera, L.A., et al., 2021. Assessment of vascular stiffness in the internal carotid artery proximal to the carotid canal in Alzheimer's disease using pulse wave velocity from low rank reconstructed 4D flow MRI. J. Cereb. Blood Flow Metab. 41, 298–311.
San-Juan, D., et al., 2017. Transcranial direct current stimulation in mesial temporal lobe epilepsy and hippocampal sclerosis. Brain Stimul. 10, 28–35.
Shin, T., Shin, W., 2020. Improved acceleration of phase-contrast flow imaging with magnitude difference regularization. Magn. Reson. Imaging 67, 1–6.
Soler, M.D., et al., 2010. Effectiveness of transcranial direct current stimulation and visual illusion on neuropathic pain in spinal cord injury. Brain. 133, 2565–2577.
Sotnikova, A., et al., 2017. Transcranial direct current stimulation modulates neuronal networks in attention deficit hyperactivity disorder. Brain Topogr. 30, 656–672.
Stagg, C.J., et al., 2013. Widespread modulation of cerebral perfusion induced during and after transcranial direct current stimulation applied to the left dorsolateral prefrontal cortex. J. Neurosci. 33, 11425–11431.
Teo, F., et al., 2011. Investigating the role of current strength in tDCS modulation of working memory performance in healthy controls. Front. Psychiatry 2, 45.
Woods, A.J., et al., 2019. Transcranial Direct Current Stimulation in Aging Research. In: Practical Guide to Transcranial Direct Current Stimulation: Principles, Procedures

and Applications. Vol., H. Knotkova, M.A. Nitsche, M. Bikson, A.J. Woods, ed.ˆeds. Springer International Publishing, Cham, pp. 569-595.
Wright, G.A., Hu, B.S., Macovski, A., 1991. 1991 I.I. Rabi Award. estimating oxygen saturation of blood in vivo with MR imaging at 1.5 T. J. Magn. Reson. Imaging 1, 275–283.
Wu, M., et al., 2019. Efficiency of repetitive transcranial direct current stimulation of the dorsolateral prefrontal cortex in disorders of consciousness: a randomized sham-controlled study. Neural Plast. 2019, 7089543.
Xu, F., Ge, Y., Lu, H., 2009. Noninvasive quantification of whole-brain cerebral metabolic rate of oxygen (CMRO2) by MRI. Magn. Reson. Med. 62, 141–148.
Yoon, E.J., et al., 2014. Transcranial direct current stimulation to lessen neuropathic pain after spinal cord injury: a mechanistic PET study. Neurorehabil. Neural Repair. 28, 250–259.
Zhao, J.M., et al., 2007. Oxygenation and hematocrit dependence of transverse relaxation rates of blood at 3T. Magn. Reson. Med. 58, 592–597.
Zhao, X., et al., 2020. Anodal and cathodal tDCS modulate neural activity and selectively affect GABA and glutamate syntheses in the visual cortex of cats. J. Physiol. 598, 3727–3745.
Zheng, X., Alsop, D.C., Schlaug, G., 2011. Effects of transcranial direct current stimulation (tDCS) on human regional cerebral blood flow. Neuroimage 58, 26–33.